A Nonlinear Attitude Estimator for Attitude and Heading Reference Systems Based on MEMS Sensors

Wang, Yunlong; Soltani, Mohsen; Hussain, Dil muhammed Akbar

Published in:
Proceedings of SICE International Symposium on Control Systems (ISCS) 2016

DOI (link to publication from Publisher):
10.1109/SICEISCS.2016.7470176

Publication date:
2016

Document Version
Early version, also known as pre-print

A Nonlinear Attitude Estimator for Attitude and Heading Reference Systems Based on MEMS Sensors

Yunlong Wang[1†] Mohsen Soltani[1] and Dil Muhammad Akbar Hussain[1]

[1]Department of Energy Technology, Aalborg University, Esbjerg, Denmark
(E-mail: way@et.aau.dk, sms@et.aau.dk, akh@et.aau.dk)

Abstract: In this paper, a nonlinear attitude estimator is designed for an Attitude Heading and Reference System (AHRS) based on Micro Electro-Mechanical Systems (MEMS) sensors. The design process of the attitude estimator is stated with detail, and the equilibrium point of the estimator error model is proved to be asymptotically stable using LaSalle's invariance set theorem through limitation of the range of scalar element of quaternion without affecting practical use. Also, a new Lyapunov candidate function, satisfying continuously differentiable positive definite requirement, is presented to avoid the problems in previous research works. Moreover, the estimation of MEMS gyroscope bias is also inclueded in this estimator. The designed nonlinear attitude estimator is firstly tested in simulation environment and then implemented in an AHRS hardware for further experiments. Finally, the attitude estimation results from the designed AHRS are compared with a high-precision commercial AHRS to validate its estimation performance.

Keywords: Nonlinear estimator, attitude estimation, MEMS sensor

1. INTRODUCTION

An Attitude Heading and Reference System (AHRS) based on Micro Electro-Mechanical Systems (MEMS) sensors, such as gyroscope, accelerometer, and magnetometer, are playing an increasingly important role in several kinds of attitude control system, such as Unmanned Aerial Vehicle (UAV) [1-3], Unmanned underwater vehicles (UUV) [4, 5]. The reason is that the MEMS sensors for AHRS are becoming much cheaper and smaller as the quick advantages of MEMS technology, which makes them quite suitable for applications requiring low cost and small size. However, relatively large measurement noise, null bias are the disadvantages of MEMS sensors. Moreover, the MEMS accelerometer can easily be affected by the vehicle acceleration and the MEMS magnetometer can be disturbed by the ferromagnetic materials around installation position. To obtain an accurate attitude estimation from measurements of MEMS sensors, an attitude estimator is needed.

Many kinds of attitude estimator have been designed, ranging from linear estimators to nonlinear estimators. The attitude estimator using standard linear Kalman filter theory can be found in [6, 7]. A much simpler kind of attitude estimator based on linear theory is linear complementary filter [8, 9], which greatly reduces the calculation time needed, compared to Kalman filter having many matrix calculation. To cope with nonlinear problems, the attitude estimator based on Extended Kalman Filter (EKF) is devised [10] through linearizing the nonlinear model by Taylor method. Especially, Multiplicative Extended Kalman Filter (MEKF) [11, 12] is a proven attitude estimation method and is widely used in low-cost AHRS. In [13], the theory based on Unscented Kalman Filter (UKF) is used on attitude estimation for faster convergence. The particle filter for attitude estimation is developed in [14] for systems with strong nonlinearity, where even EKF and UKF cannot generate acceptable estimation results. In [14], attitude estimators with the star camera measurements is developed. Recently, there are many nonlinear attitude estimators [15-18], which are designed based on nonlinear theory, such as Lyapunov method. In [19], the nonlinear complementary filter is designed, which boasts computational efficiency, easily tuned parameters, and a proof of global asymptotic stability can be found in [20]. The stability proof in [19] assumed that the reference vectors are constant, which has been relaxed by [21] to include time-varying reference vectors.

In previous research works [17, 18, 22], the $sgn(\cdot)$ function is used in the injection term of estimator. However, it is the $sgn(\cdot)$ function that causes estimator error dynamics not satisfying Lipschitz continuity condition. Satisfying Lipschitz continuity is the prerequisite of a dynamics system for stability analysis using Lyapunov theory or LaSalle's invariant set theorem [23]. In [19], the $sgn(\cdot)$ function is avoided, but the absolute function $|\tilde{s}|$ is used in Lyapunov candidate function. It is well known that $|\tilde{s}|$ does not have derivation in $\tilde{s} = 0$, so we cannot get derivation of Lyapunov candidate function in the domain including $\tilde{s} = 0$. Moreover, $\tilde{s} = 0$ is in the domain of Lyapunov candidate function in [19].

In this paper, a kind of nonlinear attitude estimator is designed and stability analysis is completed using LaSalle's invariance theorem, to solve the problems mentioned above. The design process and stability analysis are stated with detail. Moreover, the designed attitude estimator is tested in both simulation environment and hardware implementation to validate its estimation performance.

This paper is organized as follows. In Section 2, the notation and definition used is introduced. The process of designing the nonlinear attitude estimator is explained with detail in Section 3. In Section 4, the process of obtaining observed quaternion through Gauss-Newton method is explained with detail. And in Section 5, the ex-

† Yunlong Wang is the presenter of this paper.

periments and results of testing designed algorithm both in simulation and hardware environment is presented. Finally, Section 6 gives the conclusion and discussses future works.

2. NOTATION AND DEFINITIOIN

The following three different kinds of coordinate systems are used in this paper.
1. $\{n\}$, the North-East-Down reference system and is considered as the inertial coordinate system in marine research area.
2. $\{b\}$, the body-fixed reference frame.
3. $\{E\}$, attitude estimator reference frame. Mostly, there is a difference between the estimated attitude and true attitude of $\{b\}$ relative to $\{n\}$. $\{E\}$ is formed by the estimated attitude.

Quaternion is wildly used in the area of attitude estimation, as it possesses plenty of advantages, such as free singularity when pitch reaches $\pm 90\ deg$. Moreover, it is especially suitable to be implemented in Micro Controller Unit(MCU), such as ARM chip, as it requires little computational resources compared to sinusoidal function. Quaternion consists of one real part η and three imaginary parts given by a vector $\boldsymbol{\varepsilon} = [\varepsilon_1, \varepsilon_2, \varepsilon_3]^T$, and is expressed as

$$\boldsymbol{q} = [\eta, \boldsymbol{\varepsilon}^T]^T = [\eta, \varepsilon_1, \varepsilon_2, \varepsilon_3]^T$$

A unit quaternion is used to denote rotation and satisfies $\boldsymbol{q}^T\boldsymbol{q} = 1$, that is, $\|\boldsymbol{q}\|^2 = \eta^2 + \varepsilon_1^2 + \varepsilon_2^2 + \varepsilon_3^2 = 1$. According to Euler's theorem on rotation, a vector in one reference frame can be transformed to another reference frame by a simple rotation, that is, by rotation θ about a unit vector $\boldsymbol{v} = [v_1, v_2, v_3]^T$. This rotation can be defined as a unit quaternion

$$\boldsymbol{q} = \left[\ \cos(\tfrac{\theta}{2}),\quad \sin(\tfrac{\theta}{2})v_1,\quad \sin(\tfrac{\theta}{2})v_2,\quad \sin(\tfrac{\theta}{2})v_3\ \right]^T \tag{1}$$

Or as an rotation matrix

$$\begin{aligned}\boldsymbol{R}(\boldsymbol{q}) &= \boldsymbol{I}_{3\times 3} + 2\eta S(\boldsymbol{\varepsilon}) + 2S^2(\boldsymbol{\varepsilon}) \qquad (2)\\ &= \left[\begin{array}{cc} -2{\varepsilon_2}^2 - 2{\varepsilon_3}^2 + 1 & -2\,\eta\,\varepsilon_3 + 2\,\varepsilon_2\,\varepsilon_1 \\ 2\,\eta\,\varepsilon_3 + 2\,\varepsilon_2\,\varepsilon_1 & -2\,{\varepsilon_1}^2 - 2\,{\varepsilon_3}^2 + 1 \\ -2\,\eta\,\varepsilon_2 + 2\,\varepsilon_3\,\varepsilon_1 & 2\,\eta\,\varepsilon_1 + 2\,\varepsilon_3\,\varepsilon_2 \end{array}\right. \\ &\qquad \left.\begin{array}{c} 2\,\eta\,\varepsilon_2 + 2\,\varepsilon_3\,\varepsilon_1 \\ -2\,\eta\,\varepsilon_1 + 2\,\varepsilon_3\,\varepsilon_2 \\ -2\,{\varepsilon_1}^2 - 2\,{\varepsilon_2}^2 + 1 \end{array}\right] \qquad (3)\end{aligned}$$

where $\boldsymbol{R}(\boldsymbol{q}) \in SO(3)$, and

$$S(\boldsymbol{\varepsilon}) = \left[\begin{array}{ccc} 0 & -\varepsilon_3 & \varepsilon_2 \\ \varepsilon_3 & 0 & -\varepsilon_1 \\ -\varepsilon_2 & \varepsilon_1 & 0 \end{array}\right]$$

The transformation between different frames are illustrated in Fig. 1 using rotation matrix.

In Fig. 1, $\hat{\boldsymbol{q}} = [\hat{\eta}, \hat{\boldsymbol{\varepsilon}}^T]^T$, is the estimated unit quaternion obtained from attitude estimator. $\boldsymbol{q_t} = [\eta_t, \boldsymbol{\varepsilon}_t^T]^T$ is the true unit quaternion which represents the rotation from $\{b\}$ to $\{n\}$. $\tilde{\boldsymbol{q}} = [\tilde{\eta}, \tilde{\boldsymbol{\varepsilon}}^T]^T$ is the quaternion error between $\hat{\boldsymbol{q}}$ and $\boldsymbol{q_t}$ and is calculated as

$$\begin{aligned}\tilde{\boldsymbol{q}} &= \hat{\boldsymbol{q}}^{-1} \otimes \boldsymbol{q}_t \\ &= \left[\begin{array}{c} \hat{\eta}\eta_t + \hat{\boldsymbol{\varepsilon}}^T\boldsymbol{\varepsilon}_t \\ -\eta_t\hat{\boldsymbol{\varepsilon}} + \hat{\eta}\boldsymbol{\varepsilon}_t - S(\hat{\boldsymbol{\varepsilon}})\boldsymbol{\varepsilon}_t \end{array}\right]\end{aligned} \tag{4}$$

where $\otimes$ denotes quaternion multiplication. Note that all the quaternions used are unit quaternions and are normalized after calculation by $\boldsymbol{q} = \frac{\boldsymbol{q}}{\|\boldsymbol{q}\|}$. For unit quaternion, we have $\boldsymbol{q}^{-1} = \boldsymbol{q}^* = [\eta, -\boldsymbol{\varepsilon}^T]^T$, where $\boldsymbol{q}^*$ is the conjugate of $\boldsymbol{q}$. $\boldsymbol{R}(\boldsymbol{q}_t), \boldsymbol{R}(\tilde{\boldsymbol{q}}), \boldsymbol{R}(\hat{\boldsymbol{q}}) \in SO(3)$ are the rotation matrix corresponding to $\boldsymbol{q}_t, \tilde{\boldsymbol{q}}, \hat{\boldsymbol{q}}$ respectively.

The kinematic equation for a quaternion is

$$\dot{\boldsymbol{q}} = \left[\begin{array}{c} \dot{\eta} \\ \dot{\boldsymbol{\varepsilon}} \end{array}\right] = \frac{1}{2}\boldsymbol{q} \otimes \left[\begin{array}{c} 0 \\ \boldsymbol{\omega}_{b/n}^b \end{array}\right] = \boldsymbol{T_q}(\boldsymbol{q}) \cdot \boldsymbol{\omega}_{b/n}^b \tag{5}$$

where $\boldsymbol{\omega}_{b/n}^b$ denotes the rotation rate of $\{b\}$ relative to $\{n\}$, decomposed in $\{b\}$. And,

$$\boldsymbol{T_q}(\boldsymbol{q}) = \left[\begin{array}{ccc} -\varepsilon_1 & -\varepsilon_2 & -\varepsilon_3 \\ \eta & -\varepsilon_3 & \varepsilon_2 \\ \varepsilon_3 & \eta & -\varepsilon_1 \\ -\varepsilon_2 & \varepsilon_1 & \eta \end{array}\right] \tag{6}$$

is used to apply matrix multiplication, instead of quaternion multiplication, for calculation convenience.

The quaternion has to be converted into Euler angles for other system to use. This conversion is achieved by [24]

$$\begin{aligned}\varphi &= atan2(2(\hat{\varepsilon}_2 \cdot \hat{\varepsilon}_3 + \hat{\varepsilon}_1 \cdot \hat{\eta}), \hat{\eta}^2 + \hat{\varepsilon}_3^2 - \hat{\varepsilon}_2^2 - \hat{\varepsilon}_1^2) \\ \theta &= -tan^{-1}\left(\frac{2(\hat{\varepsilon}_1 \cdot \hat{\varepsilon}_3 - \hat{\varepsilon}_2 \cdot \hat{\eta})}{\sqrt{1 - 2(\hat{\varepsilon}_1 \cdot \hat{\varepsilon}_3 - \hat{\varepsilon}_2 \cdot \hat{\eta})^2}}\right) \\ \psi &= atan2(2(\hat{\varepsilon}_1 \cdot \hat{\varepsilon}_2 + \hat{\varepsilon}_3 \cdot \hat{\eta}), \hat{\eta}^2 + \hat{\varepsilon}_1^2 - \hat{\varepsilon}_2^2 - \hat{\varepsilon}_3^2)\end{aligned} \tag{7}$$

where $\hat{\eta}, \hat{\varepsilon}_1, \hat{\varepsilon}_2$, and $\hat{\varepsilon}_3$ are elements of latest estimated quaternion from nonlinear attitude estimator. ϕ, θ, ψ are the roll, pitch, and yaw respectively.

3. NONLINEAR ESTIMATOR DESIGN

In this section, the process of designing nonlinear attitude estimator is stated with detail.

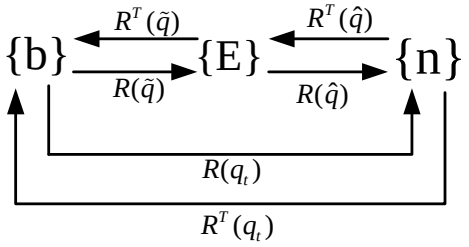

Fig. 1 Transformation between different frames using rotation matrix

3.1. Sensor model

The MEMS sensors, specifically gyroscope, accelerometer and magnetometer, are typically used to constitute an AHRS.

MEMS gyroscope measures angular velocity of $\{b\}$ relative to $\{n\}$, expressed in $\{b\}$. The model of MEMS gyroscope is

$$\boldsymbol{\omega}_{\mathrm{m}}^{b} = \boldsymbol{\omega}_{b/n}^{b} + \boldsymbol{b}_{gyro}^{b} + \boldsymbol{W}_{gyro}^{b} \in R^3 \tag{8}$$

where $\boldsymbol{\omega}_{\mathrm{m}}^{b} \in \{b\}$ denotes the rotation rate measurements of gyroscope. $\boldsymbol{\omega}_{b/n}^{b}$ is the true rotation rate. $\boldsymbol{b}_{gyro}^{b} \in \{b\}$ denotes a constant gyroscope bias. $\boldsymbol{W}_{gyro}^{b} \in \{b\}$ is zero-mean Gauss white noise.

MEMS accelerometer measures instantaneous linear acceleration $\{b\}$ minus the gravity acceleration $\boldsymbol{g}_0^n \in \{n\}$, expressed in $\{b\}$. The model of MEMS accelerometer is

$$\boldsymbol{a}_{\mathrm{m}}^{b} = \boldsymbol{R}^T(\boldsymbol{q}_t)(\dot{\boldsymbol{v}}_{m/n}^{b} - \boldsymbol{g}_0^n) + \boldsymbol{b}_{acc}^{b} + \boldsymbol{W}_{acc}^{b} \in R^3 \tag{9}$$

where $\boldsymbol{a}_{\mathrm{m}}^{b} \in \{b\}$ denotes the measurements from accelerometer. $\dot{\boldsymbol{v}}_{m/n}^{b} \in \{b\}$ is the instantaneous linear acceleration of $\{b\}$ relative to $\{n\}$. $\boldsymbol{b}_{acc}^{b}$ is the bias term, and $\boldsymbol{W}_{acc}^{b} \in \{b\}$ is zero-mean Gauss white noise.

MEMS magnetometer measures the magnetic field in $\{n\}$, expressed in b and the model is

$$\boldsymbol{m}_{m}^{b} = \boldsymbol{R}^T(\boldsymbol{q}_t)\boldsymbol{m}_{\mathrm{m}}^{n} + \boldsymbol{b}_{mag}^{b} + \boldsymbol{W}_{mag}^{b} \in R^3 \tag{10}$$

where $\boldsymbol{m}_{m}^{b} \in \{b\}$ is the measurements of magnetometer. $\boldsymbol{m}_{\mathrm{m}}^{n} \in \{n\}$ denotes the magnetic field of earth. $\boldsymbol{b}_{mag}^{b} \in \{b\}$ is the bias term and $\boldsymbol{W}_{mag}^{b} \in \{b\}$ is zero-mean Gauss white noise.

In the models above, $\boldsymbol{b}_{gyro}^{b}$ is estimated in attitude estimator and will be stated in the following contents. $\boldsymbol{b}_{acc}^{b}, \boldsymbol{b}_{mag}^{b}$ are removed by calibration for varying temperatures. $\boldsymbol{W}_{acc}^{b}, \boldsymbol{W}_{mag}^{b}$ are removed by low-pass filter. Due to the term $\dot{\boldsymbol{v}}_{m/n}^{b}$ in Eq. (9), AHRS based on accelerometers cannot work in high dynamic situations for a long time, where significant changing acceleration will seriously affect measurement accuracy of pitch and roll.

3.2. Dynamic Model of Nonlinear Attitude Estimator

The attitude dynamics model can be found by combining Eqs. (5) and (8), then

$$\begin{aligned} \dot{\boldsymbol{q}} &= \boldsymbol{T}_{\boldsymbol{q}}(\boldsymbol{q})(\boldsymbol{\omega}_{m}^{b} - \boldsymbol{b}_{gyro}^{b} - \boldsymbol{W}_{gyro}^{b}) \\ \dot{\boldsymbol{b}}_{gyro}^{b} &= 0 \end{aligned} \tag{11}$$

The following nonlinear attitude estimator model is used.

$$\begin{aligned} \dot{\hat{\boldsymbol{q}}} &= \boldsymbol{T}_{\boldsymbol{q}}(\hat{\boldsymbol{q}})[\boldsymbol{\omega}_{m}^{b} - \hat{\boldsymbol{b}}_{\boldsymbol{gyro}}^{\boldsymbol{b}} + \boldsymbol{K}_{\boldsymbol{p}} \cdot \tilde{\boldsymbol{\varepsilon}} \cdot \tilde{\eta}] \\ \dot{\hat{\boldsymbol{b}}}_{gyro}^{b} &= -\frac{1}{2}\boldsymbol{K}_{\boldsymbol{i}} \cdot \tilde{\boldsymbol{\varepsilon}} \cdot \tilde{\eta} \end{aligned} \tag{12}$$

where $\boldsymbol{K}_{\boldsymbol{p}}, \boldsymbol{K}_{\boldsymbol{i}} \in R^{3\times3}$ and $\boldsymbol{K}_{\boldsymbol{p}} > 0, \boldsymbol{K}_{\boldsymbol{i}} > 0$, are diagonal matrices, whose element values are constants parameters. $\tilde{\boldsymbol{\varepsilon}} \cdot \tilde{\eta}$ are calculated from Eq. (4). As the true quaternion, $\boldsymbol{q}_t$, is impossible to be known, the quaternion, $\boldsymbol{q}_y$, obtained from measurements of accelerometer and magnetometer through Gauss-Newton method, is used in Eq. (4).

The schematic diagram of designed nonlinear attitude estimator Eq. (12) are illustrated in Fig. 2.

In Fig. 2, the measurements from accelerometer and magnetometer are fused using Gauss-Newton method to get $\boldsymbol{q}_y$, which is then used, together with $\hat{\boldsymbol{q}}$ to calculated $\tilde{\boldsymbol{\varepsilon}} \cdot \tilde{\eta}$. As there exists measurement noise, $\boldsymbol{W}_{acc}^{b}, \boldsymbol{W}_{mag}^{b}$ in $\boldsymbol{a}_{\mathrm{m}}^{b}, \boldsymbol{m}_{\mathrm{m}}^{b}$, low-pass filter is used to remove $\boldsymbol{W}_{acc}^{b}, \boldsymbol{W}_{mag}^{b}$ from $\boldsymbol{a}_{\mathrm{m}}^{b}, \boldsymbol{m}_{\mathrm{m}}^{b}$ before they are used in Gauss-Newton method. The details of using Gauss-Newton method to get $\boldsymbol{q}_y$ can be found in Section 4. The method of converting quaternion into Euler angles can be found in Eq. (7).

The attitude estimator designed in [24],[22],[17], is similar to Eq. (12), and is put below.

$$\begin{aligned} \dot{\hat{\boldsymbol{q}}} &= \boldsymbol{T}_{\boldsymbol{q}}(\hat{\boldsymbol{q}})[\boldsymbol{\omega}_{m}^{b} - \hat{\boldsymbol{b}}_{\boldsymbol{gyro}}^{\boldsymbol{b}} + \boldsymbol{K}_{\boldsymbol{p}} \cdot \tilde{\boldsymbol{\varepsilon}} \cdot sgn(\tilde{\eta})] \\ \dot{\hat{\boldsymbol{b}}}_{gyro}^{b} &= -\frac{1}{2}\boldsymbol{K}_{\boldsymbol{i}} \cdot \tilde{\boldsymbol{\varepsilon}} \cdot sgn(\tilde{\eta}) \end{aligned} \tag{13}$$

By comparison, it can be found that term $\tilde{\boldsymbol{\varepsilon}} \cdot sgn(\tilde{\eta})$ is used in Eq. (13) instead of $\tilde{\boldsymbol{\varepsilon}} \cdot \tilde{\eta}$. It is the function $sgn(\tilde{\eta})$ that makes estimator error model Eq. (19) do not satisfy the requirement of Lipschitz continuity [23]ch4 for using Lyapunov method or LaSalle's invariance principle. So, the term $\tilde{\boldsymbol{\varepsilon}} \cdot sgn(\tilde{\eta})$ is changed into $\tilde{\boldsymbol{\varepsilon}} \cdot \tilde{\eta}$ for using LaSalle's invariance principle to analyse the stability of estimator model, which will be stated in the following contents.

3.3. Stability Analysis

Assuming $\boldsymbol{W}_{gyro}^{b} = 0$, the estimator error model, consisting of two parts, quaternion part and bias part, is obtained from Eqs. (11), (12), and (4), whose process is stated below.

From Eq. (4), we can get

$$\tilde{\boldsymbol{q}} = \begin{bmatrix} \hat{\eta}\eta + \hat{\boldsymbol{\varepsilon}}^T\boldsymbol{\varepsilon} \\ -\eta\hat{\boldsymbol{\varepsilon}} + \hat{\eta}\boldsymbol{\varepsilon} - S(\hat{\boldsymbol{\varepsilon}})\boldsymbol{\varepsilon} \end{bmatrix} \tag{14}$$

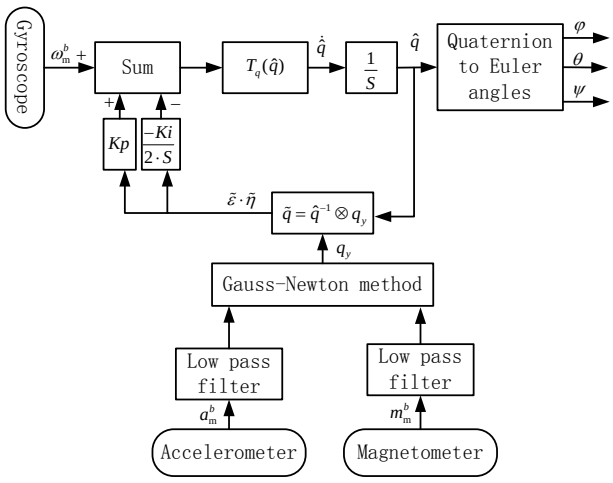

Fig. 2 Schematic diagram of nonlinear attitude estimator

$$= \begin{bmatrix} \hat{\eta}\,\eta + \hat{\varepsilon}_1\,\varepsilon_1 + \hat{\varepsilon}_2\,\varepsilon_2 + \hat{\varepsilon}_3\,\varepsilon_3 \\ \hat{\eta}\,\varepsilon_1 - \eta\,\hat{\varepsilon}_1 - \hat{\varepsilon}_2\,\varepsilon_3 + \hat{\varepsilon}_3\,\varepsilon_2 \\ \hat{\eta}\,\varepsilon_2 - \eta\,\hat{\varepsilon}_2 + \hat{\varepsilon}_1\,\varepsilon_3 - \hat{\varepsilon}_3\,\varepsilon_1 \\ \hat{\eta}\,\varepsilon_3 - \eta\,\hat{\varepsilon}_3 - \hat{\varepsilon}_1\,\varepsilon_2 + \hat{\varepsilon}_2\,\varepsilon_1 \end{bmatrix} \quad (15)$$

From Eq. (15), we can get

$$\dot{\tilde{\boldsymbol{q}}} = \begin{bmatrix} \dot{\tilde{\eta}} & \dot{\tilde{\boldsymbol{\varepsilon}}}^T \end{bmatrix}^T = \boldsymbol{M}(\eta, \dot{\eta}, \hat{\eta}, \dot{\hat{\eta}}, \boldsymbol{\varepsilon}, \dot{\boldsymbol{\varepsilon}}, \hat{\boldsymbol{\varepsilon}}, \dot{\hat{\boldsymbol{\varepsilon}}}) \quad (16)$$

where $\boldsymbol{M}(\cdot) \in R^{4\times 1}$ is so large that it will not be put here. After putting the terms $\dot{\eta}, \dot{\hat{\eta}}, \dot{\boldsymbol{\varepsilon}}, \dot{\hat{\boldsymbol{\varepsilon}}}$ obtained from Eqs. (11) and (12), into $\boldsymbol{M}(\cdot)$ and some tedious calculation, the quaternion part of estimator error model can be obtained and is

$$\dot{\tilde{\boldsymbol{q}}} = \begin{bmatrix} \dot{\tilde{\eta}} \\ \dot{\tilde{\boldsymbol{\varepsilon}}} \end{bmatrix} = \begin{bmatrix} \frac{1}{2}\tilde{\boldsymbol{\varepsilon}}^T[\tilde{\boldsymbol{b}} + \boldsymbol{K_p}\cdot\tilde{\boldsymbol{\varepsilon}}\cdot\tilde{\eta}] \\ -\frac{1}{2}[\tilde{\eta}\cdot\boldsymbol{I} + S(\tilde{\boldsymbol{\varepsilon}})]\cdot[\tilde{\boldsymbol{b}} + \boldsymbol{K}_p\cdot\tilde{\boldsymbol{\varepsilon}}\cdot\tilde{\eta}] \end{bmatrix} \quad (17)$$

The bias part of estimator model is got through $\tilde{\boldsymbol{b}} = \boldsymbol{b}^b_{gyro} - \hat{\boldsymbol{b}}^b_{gyro}$, then

$$\begin{aligned} \dot{\tilde{\boldsymbol{b}}} &= \dot{\boldsymbol{b}}_{gyro} - \dot{\hat{\boldsymbol{b}}}_{gyro} \\ &= \frac{1}{2}\boldsymbol{K}_i\cdot\tilde{\eta}\cdot\tilde{\boldsymbol{\varepsilon}} \end{aligned} \quad (18)$$

Finally, put Eqs. (17) and (18) together, the estimator error model is

$$\begin{bmatrix} \dot{\tilde{\eta}} \\ \dot{\tilde{\boldsymbol{\varepsilon}}} \\ \dot{\tilde{\boldsymbol{b}}} \end{bmatrix} = \begin{bmatrix} \frac{1}{2}\tilde{\boldsymbol{\varepsilon}}^T[\tilde{\boldsymbol{b}} + \boldsymbol{K}_p\cdot\tilde{\boldsymbol{\varepsilon}}\cdot\tilde{\eta}] \\ -\frac{1}{2}[\tilde{\eta}\cdot\boldsymbol{I} + S(\tilde{\boldsymbol{\varepsilon}})]\cdot[\tilde{\boldsymbol{b}} + \boldsymbol{K}_p\cdot\tilde{\boldsymbol{\varepsilon}}\cdot\tilde{\eta}] \\ \frac{1}{2}\boldsymbol{K}_i\cdot\tilde{\boldsymbol{\varepsilon}}\cdot\tilde{\eta} \end{bmatrix} \quad (19)$$

By setting the right part of Eq. (19) to be zero, together with $\tilde{\eta}^2 + \tilde{\boldsymbol{\varepsilon}}^2 = 1$ as $\|\tilde{\boldsymbol{q}}\| = 1$, the equilibrium points of estimator error model can be obtained and is, $\tilde{\boldsymbol{q}}_{\boldsymbol{0}} = [\tilde{\eta}_0, \tilde{\boldsymbol{\varepsilon}}_0^T]^T = [\pm 1\ 0\ 0\ 0]^T$.

The Lynapunov candidate function used is

$$V = \frac{1}{2}\tilde{\boldsymbol{b}}^T\cdot\boldsymbol{K_i}^{-1}\cdot\tilde{\boldsymbol{b}} + (\frac{1}{2} - \frac{1}{2}\tilde{\eta}^2) \quad (20)$$

It can be easily verified that V is a continuously differentiable positive definite function in the domain of estimator error model.

Then, we have

$$\begin{aligned} \dot{V} &= \frac{1}{2}\left(\dot{\tilde{\boldsymbol{b}}}^T\boldsymbol{K_i}^{-1}\tilde{\boldsymbol{b}} + \tilde{\boldsymbol{b}}^T\boldsymbol{K_i}^{-1}\dot{\tilde{\boldsymbol{b}}}\right) - \tilde{\eta}\dot{\tilde{\eta}} && (21) \\ &= \frac{1}{2}\tilde{\eta}\tilde{\boldsymbol{\varepsilon}}^T\tilde{\boldsymbol{b}} - \tilde{\eta}\cdot\frac{1}{2}\boldsymbol{\varepsilon}^T\left(\tilde{\boldsymbol{b}} + \boldsymbol{K_p}\tilde{\boldsymbol{\varepsilon}}\tilde{\eta}\right) && (22) \\ &= -\frac{1}{2}\tilde{\eta}^2\tilde{\boldsymbol{\varepsilon}}^T\boldsymbol{K_p}\tilde{\boldsymbol{\varepsilon}} \le 0 && (23) \end{aligned}$$

From Eq. (1), it can be known that $\tilde{\eta}_0 = \pm 1$ means $\theta = 0$ or 2π. So, it is reasonable to limit the rotation angle between two reference frames in $(-2\pi, 2\pi)$. Then, $\tilde{\eta} \in (-1, 1]$ and the equilibrium point of estimator error model Eq. (19) is only $\tilde{\boldsymbol{q}}_{\boldsymbol{0}} = [1, 0, 0, 0]^T$.

Next, LaSalle's invariance set theorem is applied to prove that the equilibrium point $\tilde{\boldsymbol{q}}_{\boldsymbol{0}}$ of Eq. (19) is locally asymptotically stable.

Firstly, the neighbourhood of $\tilde{\boldsymbol{q}}_{\boldsymbol{0}}$ is defined as,

$$\begin{aligned} D &= \left\{\left(\tilde{\eta}, \tilde{\boldsymbol{\varepsilon}}, \tilde{\boldsymbol{b}}\right) | -1 < \tilde{\eta} \le 1, \tilde{\eta}^2 + \tilde{\boldsymbol{\varepsilon}}^2 = 1,\right. \\ &\quad \left.\tilde{\eta} \in R, \tilde{\boldsymbol{\varepsilon}} \in R^3, \tilde{\boldsymbol{b}} \in R^3\right\} \end{aligned} \quad (24)$$

From the above analysis, it is easily found that, in D, the Lyapunov function $V : D \to R$ is a continuously differentiable positive definite function, containing the equilibrium point $\tilde{\boldsymbol{q}}_{\boldsymbol{0}}$, and $\dot{V} \le 0$ in D. Define $S = \{(\tilde{\eta}, \tilde{\boldsymbol{\varepsilon}}, \tilde{\boldsymbol{b}}) \in D | \dot{V} = 0\}$ and we can find that only $\tilde{\boldsymbol{q}}_0$ stay identically in D. According to Corollary 4.1 in [23], $\tilde{\boldsymbol{q}}_0$ is asymptotically stable. Furthermore, D is the domain of attraction of $\tilde{\boldsymbol{q}}_0$.

4. OBSERVED QUATERNION

In this section, the observed quaternion $\boldsymbol{q}_y$ is obtained from measurements of accelerometer and magnetometer through Gauss-Newton method [7, 8].

First of all, the reference vectors of accelerometer and magnetometer are introduced. When AHRS is put in zero orientation, the measurements of accelerometer and magnetometer can be read from sensor registers, the normalization of which are taken as the reference of accelerometer and magnetometer respectively. Note that the zero orientation is when the $x - y$ plane of AHRS is in the horizontal plane, the direction of z axis of AHRS is the same as that of acceleration of gravity, and the direction of x axis of AHRS is the same as that of horizontal component of geomagnetic field. Then, the reference vector is $\boldsymbol{a}_r = [0\ 0\ 1]^T$ for accelerometer, and is $\boldsymbol{m}_r = [mx_r\ 0\ mz_r]^T$ for magnetometer, where mx_r, mz_r are constants and are the normalized measurements of magnetometer when AHRS is in zero orientation. The reason that $my_r = 0$ is the x axis of AHRS points to the direction of geomagnetic field.

After getting reference vectors of accelerometer and magnetometer, the rotation models of accelerometer and magnetometer are expressed as

$$\boldsymbol{a}_r = \boldsymbol{R}(\boldsymbol{q})\cdot\boldsymbol{a}^b_m \quad (25)$$

$$\boldsymbol{m}_r = \boldsymbol{R}(\boldsymbol{q})\cdot\boldsymbol{m}^b_m \quad (26)$$

where $\boldsymbol{a}^b_m, \boldsymbol{m}^b_m$ are the current reading from accelerometer and magnetometer.

The observed quaternion, $\boldsymbol{q}_y$, is obtained by minimizing the following error equations using Gauss-Newton method.

$$\begin{aligned} \boldsymbol{E}_{am}(\boldsymbol{q}_y)_{6\times 1} &= \begin{bmatrix} \boldsymbol{E}_{a,3\times 1} \\ \boldsymbol{E}_{m,3\times 1} \end{bmatrix} \\ &= \begin{bmatrix} \boldsymbol{R}(\boldsymbol{q}_y) & \boldsymbol{0}_{3\times 3} \\ \boldsymbol{0}_{3\times 3} & \boldsymbol{R}(\boldsymbol{q}_y) \end{bmatrix}\begin{bmatrix} \boldsymbol{a}^b_m \\ \boldsymbol{b}^b_m \end{bmatrix} \\ &\quad - \begin{bmatrix} \boldsymbol{a}_r \\ \boldsymbol{m}_r \end{bmatrix} \end{aligned} \quad (27)$$

Note that the four elements of $\boldsymbol{q}_y$ form $\boldsymbol{R}(\boldsymbol{q}_y)$, which can be found in Eq. (2).

The cost function is

$$S = \frac{1}{2}\|\boldsymbol{E}_{am}(\boldsymbol{q}_y)\|^2 \tag{28}$$

where $\|\cdot\|$ is the L^2 norm.

$\boldsymbol{q}_y$ is found through recursion. In iteration $k+1$, through Taylor expansion method, we can get

$$\begin{aligned}\boldsymbol{E}_{am}(\boldsymbol{q}_y(k+1)) &= \boldsymbol{E}_{am}(\boldsymbol{q}_y(k)+\Delta\boldsymbol{q}_y)\\ &= \boldsymbol{E}_{am}(\boldsymbol{q}_y(k))+\boldsymbol{J}\cdot\Delta\boldsymbol{q}_y\end{aligned} \tag{29}$$

where $\Delta\boldsymbol{q}_y = \boldsymbol{q}_y(k+1)-\boldsymbol{q}_y(k)$, $\boldsymbol{J}$ is the Jacobian matrix, and is

$$\boldsymbol{J} = \left.\frac{\partial \boldsymbol{E}_{am}(\boldsymbol{q}_y)}{\partial \boldsymbol{q}_y}\right|_{\boldsymbol{q}_y=\boldsymbol{q}_y(k)}$$

Then,

$$\begin{aligned}S &= \frac{1}{2}\|\boldsymbol{E}_{am}(\boldsymbol{q}_y(k+1))\|^2\\ &= \frac{1}{2}(\boldsymbol{E}_{am}(\boldsymbol{q}_y(k+1)))^T\cdot(\boldsymbol{E}_{am}(\boldsymbol{q}_y(k+1)))\\ &= \frac{1}{2}(\boldsymbol{E}_{am}(\boldsymbol{q}_y(k))+\boldsymbol{J}\cdot\Delta\boldsymbol{q}_y)^T\\ &\quad\cdot(\boldsymbol{E}_{am}(\boldsymbol{q}_y(k))+\boldsymbol{J}\cdot\Delta\boldsymbol{q}_y)\\ &= \frac{1}{2}\boldsymbol{E}_{am}(\boldsymbol{q}_y(k))^T\boldsymbol{E}_{am}(\boldsymbol{q}_y(k))\\ &\quad+\frac{1}{2}(\boldsymbol{q}_y(k+1)-\boldsymbol{q}_y(k))^T\cdot\boldsymbol{J}^T\cdot\boldsymbol{J}\\ &\quad\cdot(\boldsymbol{q}_y(k+1)-\boldsymbol{q}_y(k))\\ &\quad+\boldsymbol{E}_{am}(\boldsymbol{q}_y(k))^T\cdot\boldsymbol{J}\cdot(\boldsymbol{q}_y(k+1)-\boldsymbol{q}_y(k))\end{aligned} \tag{30}$$

Then,

$$\frac{\partial S}{\partial \boldsymbol{q}_y(k+1)} = \boldsymbol{J}^T\cdot\boldsymbol{J}\cdot(\boldsymbol{q}_y(k+1)-\boldsymbol{q}_y(k))+\boldsymbol{J}^T\cdot\boldsymbol{E}_{am}(\boldsymbol{q}_y(k))$$

By setting $\frac{\partial S}{\partial \boldsymbol{q}_y(k+1)}=0$, the update of $\boldsymbol{q}_y$ is obtained

$$\begin{aligned}\boldsymbol{q}_y(k+1) &= \boldsymbol{q}_y(k)-(\boldsymbol{J}^T\cdot\boldsymbol{J})^{-1}\cdot\boldsymbol{J}^T\cdot\boldsymbol{E}_{am}(\boldsymbol{q}_y(k))\\ \boldsymbol{q}_y(k+1) &= \frac{\boldsymbol{q}_y(k+1)}{\|\boldsymbol{q}_y(k+1)\|}\end{aligned} \tag{31}$$

Note that, $\boldsymbol{q}_y$ has to be normalized after each update step to make it be a unit quaternion for rotation representation. The convergence of $\boldsymbol{q}_y$, using Gauss-Newton method, can be found in Fig. 3.

5. SIMULATION AND HARDWARE IMPLEMENTATION

To validate the performance of designed nonlinear attitude estimator, it is firstly tested in simulation environment and then implemented in AHRS hardware for further test.

The simulation system of nonlinear attitude estimator is built in Simulink and mainly consists of two parts, one is the algorithm itself which are stated with detail in previous sections, and the other one is about generating MEMS sensor measurements, whose schematic diagram is shown in Fig. 4.

In Fig. 4, sinusoidal functions are used as the signals of rotation rate of $\{b\}$ relative to $\{n\}$, which are then overlapped with zero-mean Gauss white noise and added with the gyroscope biases to finally form the measurements of gyroscope. $p,q,r\in\{b\}$ need to be transformed into $\{n\}$ through $T_b^n(\varphi,\theta,\psi)$, before being integrated to get $\varphi,\theta,\psi\in\{n\}$. The accelerator reference vector $[0,0,1]^T$ and magnetometer reference vector $[mx,0,mz]^T$ are the normalized values of measurements of accelerometer and magnetometer respectively when they are in zero orientation, that is, $\varphi=0,\theta=0,\psi=0$. These reference vectors are in $\{n\}$ and are transformed into $\{b\}$, which are then overlapped with zero-mean Gauss white noise to get the measurements of accelerometer and magnetometer respectively. The specific value of matrices, $T_b^n(\varphi,\theta,\psi)$ and $R_n^b(\varphi,\theta,\psi)$ can be found in [24]ch2 and are different from the terms in Eqs. (2) and (6), where quaternion is used, but here it is the Euler angles that are used. The variances of measurements of MEMS sensors for generating zero-mean Gauss white noise are obtained through recording sensor measurements from AHRS hardware. The running frequency

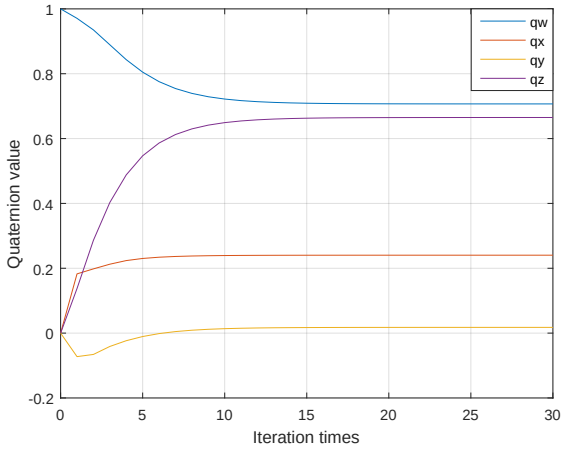

Fig. 3 Convergence of q_y using Gauss-Newton method

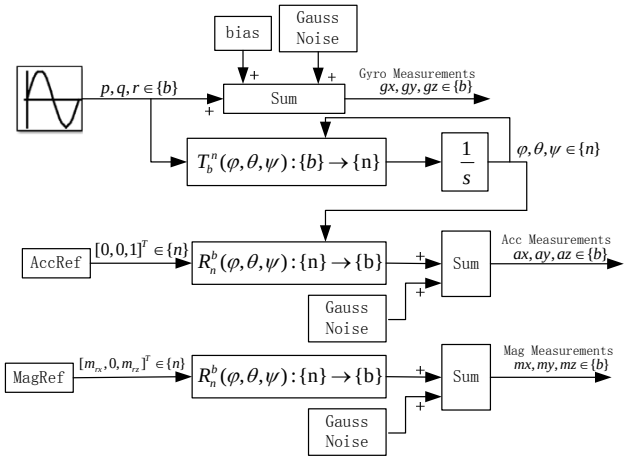

Fig. 4 Schematic diagram of generating measurements of MEMS sensors

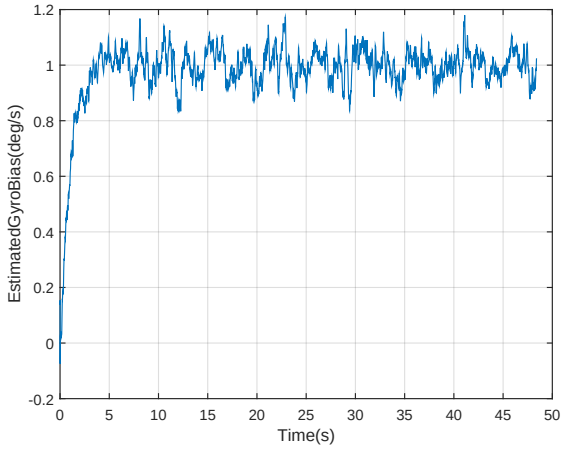

Fig. 5 Gyroscope bias estimaiton with true bias 1.0 deg/s

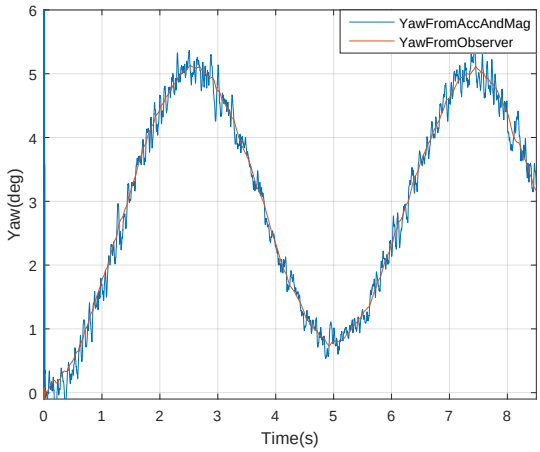

Fig. 6 Simulation results of yaw

of the simulation system is 1 KHz, and the amplitude of sinusoidal function, representing the rotation rate of roll, pith and yaw is 3 deg/s. The periods of sinusoidal functions of roll, pith and yaw are 10 s, 10 s, and 5 s respectively.

The bias of gyroscope is set to be 1.0 deg/s during simulation, and the estimated bias is gradually converged to the true value, as shown in Fig. 5.

To avoid too many figures, only the estimation result of yaw is present, as shown in Fig. 6, which is similar to that of roll and pitch. In Fig. 6, the blue line represents the yaw obtained from measurements of accelerometer and magnetometer directly by using Gauss-Newton method. Although low-pass filter is used to filter out the high-frequency noise in measurements of accelerometer and magnetometer, the vibration of yaw result, obtained directly from measurements of accelerometer and magnetometer, can clearly be seen from the blue curve in Fig. 6. Meanwhile, the red curve in Fig. 6, representing the yaw result from nonlinear attitude estimator fusing measurements of three MEMS sensors together, is much smoother, compared to the blue curve.

After successful simulation test, the designed algorithm is further tested in designed AHRS hardware, whose hardware picture is shown in Fig. 7

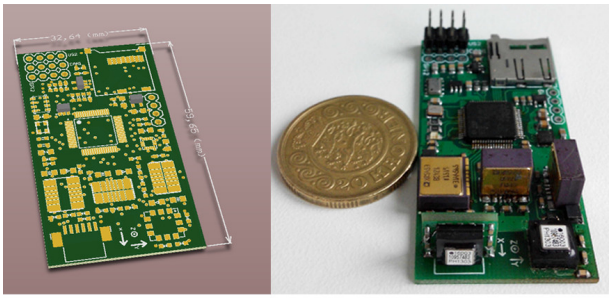

(a) (b)

Fig. 7 (a) Designed PCB of AHRS, (b) AHRS hardware

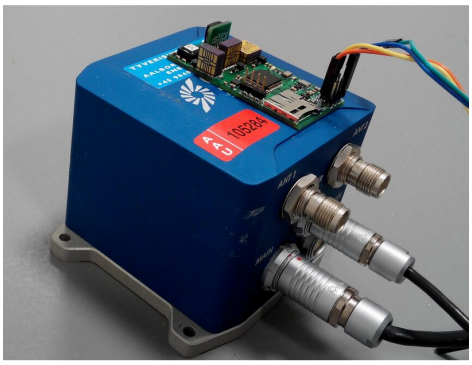

Fig. 8 Placement of designed AHRS and commercial AHRS

The Printed Circuit Board (PCB) of designed AHRS is depicted in Fig. 7(a). To decrease the size of AHRS hardware, this PCB is designed to be with 4 layers. The final size of AHRS hardware is about 33*60 mm, which is only a little larger than a coin, as shown in Fig. 7(b). The main electronic components in AHRS hardware are ARM chip, MEMS gyrosocpe, accelerometer and magnetometer.

The designed AHRS is mounted together with a high-precision commercial AHRS to compare the real-time running results between them, as shown in Fig. 8. The precision of commercial AHRS is 0.05 deg for roll and pitch, and 0.5 deg for yaw when using magnetometer or 0.05 deg for yaw when using dual antenna GPS to correct yaw error in gyroscope.

The comparison results of roll, pitch and yaw between designed AHRS and commercial AHRS are shown in Fig. 9, Fig. 10, Fig. 11, respectively.

From Fig. 9 to Fig. 11, it can be seen that the designed nonlinear attitude estimator can track the true attitude from commercial AHRS and the stability of designed nonlinear attitude estimator is also validated through hardware experiments. The estimation error of roll and pitch are within 0.2 deg during static stage or stage with slow rotation speed. The errors of roll and pitch are within 0.5 deg during stage with high rotation

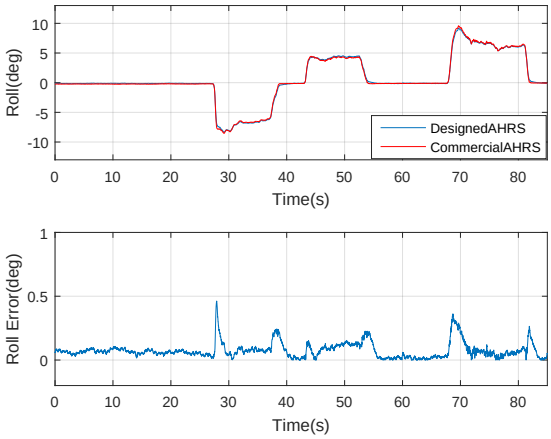

Fig. 9 Comparison of roll between designed AHRS and commercial AHRS

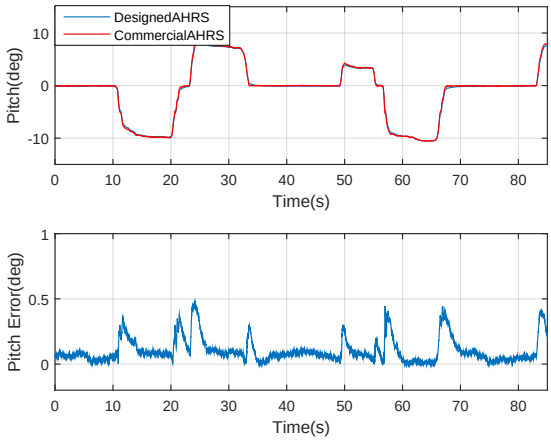

Fig. 10 Comparison of pitch between designed AHRS and commercial AHRS

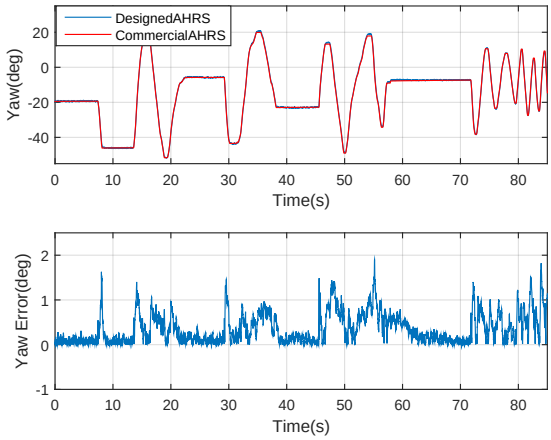

Fig. 11 Comparison of yaw between designed AHRS and commercial AHRS

speed, 15 deg/s exactly. The estimation error of yaw is relatively large, compared to that of roll and pitch, and is within 0.5 deg during static stage. During rotation stage, the error of yaw are within 2.0 deg. The reason yaw accuracy is relatively lower is that the magnetometer is not easy to be calibrated and can be easily affected by the ferromagnetic materials in laboratory.

6. CONCLUSIONS AND FUTURE WORKS

A nonlinear attitude estimator is designed based on previous research works for an MEMS sensors based AHRS. The process of design is explained with detail and the stability of nonlinear attitude estimator is proved using LaSalle's invariance set theorem in the condition of limiting the range of the scalar element of error quaternion. Also, a new kind of Lyapunov candidate function, satisfying continuously differentiable positive definite requirement, is presented to avoid the problems in previous research works. The process of getting observed quaternion is explained with detail. The designed algorithm is tested under simulation and hardware environments to validate its estimation performance. From the simulation results, it is shown that the MEMS gyroscope bias can be correctly estimated. From the results of hardware tests, it is shown that the algorithm is stable during different stages and can estimate the true attitude from commercial AHRS. The estimation accuracy is 0.5 deg for roll and pitch, 2.0 deg for yaw in all testing scenarios.

There is still potential in designed AHRS for higher estimation accuracy, which needs further researches in calibration of MEMS sensors, especially magnetometer, as it can be easily affected by ferromagnetic materials around. Another point that will be improved is the increase of algorithm cycle frequency. Further optimization works will be done to increase its cycle frequency from current 1KHz to 2KHz to increase attitude estimation accuracy.

REFERENCES

[1] S. Barros dos Santos, C. Nascimento, S. Givigi, T. Mercante, and N. de Oliveira, "Implementation of a real-time attitude system for the stabilization control of a quad-rotor robot," in *Systems Conference (SysCon), 2013 IEEE International*, April 2013, pp. 387–393.

[2] M. Cordoba, "Attitude and heading refernce system i-ahrs for the efigenia autonomous unmanned aerial vehicles uav based on mems sensor and a neural network strategy for attitude estimation," in *Control Automation, 2007. MED '07. Mediterranean Conference on*, June 2007, pp. 1–8.

[3] R. Lima and L. Torres, "Performance evaluation of attitude estimation algorithms in the design of an ahrs for fixed wing uavs," in *Robotics Symposium and Latin American Robotics Symposium (SBR-LARS), 2012 Brazilian*, Oct 2012, pp. 255–260.

[4] N. Y. Ko and S. Jeong, "Attitude estimation and dvl based navigation using low-cost mems ahrs for uuvs," in *Ubiquitous Robots and Ambient Intelli-*

gence (URAI), 2014 11th International Conference on, Nov 2014, pp. 605–607.

[5] G. Troni and L. Whitcomb, "Experimental evaluation of a mems inertial measurements unit for doppler navigation of underwater vehicles," in *Oceans, 2012*, Oct 2012, pp. 1–7.

[6] D. Comotti, M. Ermidoro, M. Galizzi, and A. Vitali, "Development of a wireless low-power multi-sensor network for motion tracking applications," in *Body Sensor Networks (BSN), 2013 IEEE International Conference on*, May 2013, pp. 1–6.

[7] Y. Wang, A. Hussain, and M. Soltani, "A mems-based adaptive ahrs for marine satellite tracking antenna," in *10th Conference on Manoeuvring and Control of Marine Craft*, 2015.

[8] D. Comotti, "Orientation estimation based on gauss-newton method and implementation of a quaternion complementary filter," 2011.

[9] E. Bachmann, I. Duman, U. Usta, R. Mcghee, X. Yun, and M. Zyda, "Orientation tracking for humans and robots using inertial sensors," in *Computational Intelligence in Robotics and Automation, 1999. CIRA '99. Proceedings. 1999 IEEE International Symposium on*, 1999, pp. 187–194.

[10] J. Marins, X. Yun, E. Bachmann, R. McGhee, and M. Zyda, "An extended kalman filter for quaternion-based orientation estimation using marg sensors," in *Intelligent Robots and Systems, 2001. Proceedings. 2001 IEEE/RSJ International Conference on*, vol. 4, 2001, pp. 2003–2011.

[11] Y. C. John L. Crassidis, F. Landis Markley, "A survey of nonlinear attitude estimation methods," *Journal of Guidance, Control, and Dynamics*, vol. Vol. 30, no. No. 1, pp. pp. 12–28, 2007.

[12] F. L. Markley, "Attitude error representations for kalman filtering," *Journal of Guidance, Control, and Dynamics*, vol. Vol. 26, no. No. 2, pp. pp. 311–317, 2003.

[13] F. L. M. John L. Crassidis, "Unscented filtering for spacecraft attitude estimation," *Journal of Guidance, Control, and Dynamics*, vol. Vol. 26, no. No. 4, pp. pp. 536–542, 2003.

[14] Y. Cheng and J. L. Crassidis, "Particle filtering for sequential spacecraft attitude estimation," in *AIAA Guidance, Navigation, and Control Conference*, 2004, pp. 04–5337.

[15] F. L. Markley, J. L. Crassidis, and Y. Cheng, "Nonlinear attitude filtering methods," vol. 1, 2005, pp. 753 – 784.

[16] H. Nijmeijer and T. Fossen, *New Directions in Nonlinear Observer Design*, ser. Lecture Notes in Control and Information Sciences. Springer London, 1999.

[17] B. Vik and T. Fossen, "A nonlinear observer for gps and ins integration," in *Decision and Control, 2001. Proceedings of the 40th IEEE Conference on*, vol. 3, 2001, pp. 2956–2961 vol.3.

[18] J. Thienel and R. Sanner, "A coupled nonlinear spacecraft attitude controller and observer with an unknown constant gyro bias and gyro noise," *Automatic Control, IEEE Transactions on*, vol. 48, no. 11, pp. 2011–2015, Nov 2003.

[19] R. Mahony, T. Hamel, and J.-M. Pflimlin, "Nonlinear complementary filters on the special orthogonal group," *IEEE Transactions on Automatic Control*, vol. 53, no. 5, pp. 1203 – 1218, 2008.

[20] K. J. Jensen, "Generalized nonlinear complementary attitude filter," *Journal of Guidance, Control, and Dynamics*, vol. 34, no. 5, pp. 1588–1593, 2011.

[21] H. Grip, T. Fossen, T. Johansen, and A. Saberi, "Attitude estimation using biased gyro and vector measurements with time-varying reference vectors," *Automatic Control, IEEE Transactions on*, vol. 57, no. 5, pp. 1332–1338, May 2012.

[22] B. Vik and T. I. Fossen, "A nonlinear observer for integration of gps and inertial navigation systems," *Modeling, Identification and Control*, vol. 21, no. 4, pp. 192–208, 2000.

[23] H. K. Khalil, *Nonlinear Systems (3rd Edition)*. Prentice Hall, 2002, chapter 4.

[24] T. I. Fossen, *Handbook of Marine Craft Hydrodynamics and Motion Control*. Wiley, 2011.